Management Systems in Production Engineering

2026, Volume 34, Issue 1, pp. 1-13

Date of submission of the article to the Editor: 02/2025
Date of acceptance of the article by the Editor: 01/2026

DOI 10.2478/mspe-2026-0001

EXPERIMENTAL STUDY OF THE EFFECTIVENESS OF Al_2O_3-SiO_2 NPMEDM FOR SURFACE TOPOGRAPHY OF STAINLESS STEEL 304L

Qasim Abdulameer Sachit, Maan Abed Tawfiq
University of Technology

Osam Hassan Attia
University of Baghdad

Mohanad Jameel Zghair
Midland Refineries Company

Abstract:
Among the several machining techniques used in mold and die manufacture, electro-discharge machining (EDM) is a unique type of machining. One of the most recent developments in thermo-electric processes is nano powder-mixed electric discharge machining (NPMEDM), which involves suspending metallic nano powder in a dielectric. The purpose of this work is to investigate the effects on surface topography (outputs) of Al_2O_3-SiO_2 nano powders mixture, which were selected from several mixtures or individual nano powders, after reviewing previous research, as nano powder concentration and nano powder mixing ratio. At concentrations of (1, 2, 3, 4, 5 g/l) mixed into the dielectric fluid of EDM on stainless steel 304L, with a mixing rate that varies for each mixture from 30% to 70%, achieving 100% for the mixture as a whole with an interval of 10% at each level. Other electric parameters (inputs) include pulse on time (50, 100, 150, 200, 250 µs), current (20, 25, 30, 35, 40 A), and pulse off time (25, 50, 75, 100, 125 µs). Response Surface Methodology (RSM) has been utilized to determine the mathematical relationship between the input and output and the NPMEDM process. White Layer Thickness (WLT), Heat Affected Zone (HAZ), and Surface Crack Density (SCD) are used to gauge the effectiveness of the machining process. The experiments were conducted using 50 experiments using the Design Expert 11 program and Central Composite Design (CCD) methodology. The results obtained were analyzed to determine the extent of the influence of the inputs on the response of the stainless steel 304L surface; we received an improvement in surface response, decreasing WLT, HAZ, and SCD by 5.8%, 17.7%, and 2.6%, respectively.

Key words: electrical discharge machining, Al_2O_3 nano powder, SiO_2 nano powder, stainless steel 304l

INTRODUCTION

Stainless steel 304L, one of the most difficult materials, is the subject of the current investigation. The workpiece may experience internal stress, and the tool may sustain damage if this material is processed using conventional methods. This problem is resolved by milling the stainless steel 304L using electrical discharge machining (EDM). This study seeks to decrease the white layer thickness, heat-affected zone, and surface crack density by optimizing input process parameters. An electrode made of copper wire was employed in this experiment. The experiment's findings show that the thickness of the machined surface white layer decreases when aluminum oxide and silicon dioxide nano powder are added to the dielectric. HAZ has decreased, and SCD has significantly improved. The material removal process in NPMEDM and conventional EDM are different. The effect of adding nano powder into the dielectric medium produce higher MRR than traditional EDM. The mechanism of NPMEDM and stated that when applying the potential difference between the tool and the workpiece. The suspended nano powder particles into the dielectric medium get energized and move in a zig-zag path. Due to the potential difference, powder particles align themselves in the form of bridge between tool and machining area. This chain type arrangement helps the powder particles to form chain mechanisms like a bridge between the electrodes. Due to the gap voltage, the bridging effect and insulating strength of the dielectric

fluid decrease resulting in a short circuit which causes an early discharge in the spark gap. Therefore, a series of discharge is obtained. It is further investigated and found that an increase in discharge frequency generates more sparks within the machining area. Therefore, more material removed from the work surface. The added powder particles also enlarge the plasma channel by increasing the spark gap also widen it. The sparks generated are uniformly distributed over the machined surface. Therefore, material removed from the machined surface is uniformly and form shallow craters. The uniformly distributed sparks improve the morphology of the machined surface.

LITERATURE REVIEW

Introduced SiO_2 and Al_2O_3 particles in nano size to the dielectric solution used in powder electric discharge machining (PEDM) to study the effect of these adding on the machining process and surface quality of Ti-6Al-4V alloy for biomedical applications. MRR, TWR, integrity of the treated material, and surface roughness were examined in this research. SEM scanning confirmed that the resulting surface quality improved and decreased the crack rate and heat-affected zone (HAZ) [1]. Studied the effect of graphite powder addition, concentration, and manufacturing parameters on the surface quality produced by the PMEDM process of a nickel-based superalloy (Inconel 625). They study the surface roughness (Ra), surface crack density (SCD), layer thickness, whiteness, microhardness depth profile, potential phase changes, and residual stress. Researchers explained this improvement is due to the large distribution area of discharge energy caused by the powder particles. So, craters of shallow and large sizes are formed on the surface of the workpiece. Thus, the gas entrapping is reduced in the cavities. On the other hand, the formation of carbides and other alloy compounds is responsible for increasing the hardness in the surface and subsurface areas [2]. Studied machining parameters such as powder concentration, peak current, duty cycle, gap voltage, and pulse time to compare conventional (EDM) process with (PEDM) when machining Inconel 625. Also, the effect of powder concentration was studied in this study. Surface integrity improved by adding the powder compared with the conventional (EDM) technique. The lowest surface roughness, residual stresses, and the highest microhardness were obtained by adding silicon powder [3]. Studied the machining process of 316L stainless steel using the EDM process. The researchers investigated the effect of adding TiO_2 nanoparticles, tungsten electrodes, and different manufacturing process parameters on machining. The MRR was enhanced to 6.75 mg/min by raising the current value to 28A. This improvement can be attributed to transferring the heat energy to the gap between the electrode and the workpiece. About the SR, smaller machining parameters introduced better SR. The higher values of machining parameters result in high energy, a powerful explosion, deep craters, and increased SR. X-ray diffraction and SEM scanning confirmed that the resulting surface quality improved, and the crack rate decreased compared to the traditional EDM technique [4]. Explained the effect of adding graphite and alumina powders to the dielectric solution to study the impact of these additions on the machining quality of the PMEDM process. This study studied surface roughness, crack depth, waviness, fracture density, microhardness, residual stress, and recast layer thickness. The results showed that the addition of both graphite and alumina powders resulted in an improvement in surface roughness, while other parameters, crack depth (C_d), recast layer thickness (RTL), and surface crack density (SCD) improved only by adding graphite powder during PMEDM process, this may because of the uniform spark distribution in the graphite. The results also showed that these additions increased the machined profile's taper and WTR [5]. Studied the effect of adding Al_2O_3 particles in various micro sizes to the dielectric solution (kerosene) in the EDM process on the surface quality and manufacturing conditions of Ti-6Al-4V alloy. The results showed higher MRR by adding micron powders with a ratio of 2.5 g/l, and this concentration resulted in lower TWR. Then MRR and TWR were reduced with 5 g/l concentration. On the other hand, the surface quality improved by adding Al_2O_3 powder compared with pure kerosene. This addition led to the ionization of the water-soluble anionic chemical emulsifier present in the kerosene, resulting in a rise in the total electrical conductivity of the dielectric [6]. studied the effect of using emulsified water, a mixture of water, emulsifier, and machine oil, as a dielectric solution compared to pure kerosene. The results showed an increasing MRR of around 34%, an improvement in surface quality of about 25%, and 150 µm layer thickness with 1600 HV of hardness compared with pure kerosene. The rise in the total electrical conductivity of the dielectric may be attributed to the ionization of the water-soluble anionic chemical emulsifier present in the emulsified oil [7]. Studied the effect of some important parameters such as polarity, electrode type, peak current, pulse on time, duty cycle, voltage gap, back-off distance, and powder concentration on the machining of Inconel 718 using an electrical discharge process with fine graphite powder mixed dielectric liquid. The results showed a significant improvement in TWR with the following parameters: I = 0.5 A, T_{on} += 150 µs, V_{gap} = 40 V, and duty cycle = 0.87. Also, the WR enhanced with the following parameters: I = 6 A, T_{on} = 150 ms, V_{gap} = 40 V, and duty cycle = 0.87. Using a copper electrode. On the other hand, the S/N ratio for TWR and WR had a grade of 7.9590 dB and 6.0422 dB, respectively [8]. Investigated the effect of adding tantalum carbide (TaC) nano powder (25.00 g/l) to kerosene as dielectric fluid on the stainless steel machined using EDM. I_p, T_{on}, and T_{off} were studied as machining parameters. The results showed that the machined surface of samples contained elements produced from TaC powder. The microhardness value was 1,200 HV, 1.5 times that of conventional EDM. Improvement in weight loss in corrosion test values was 0.056 µg/min for the PEDM process while 10.56 µg/min for conventional EDM [9]. examined the discharge parameters of surface strengthening using PEDM of H13 steel. YG8 Tungsten Carbide was used as an electrode, nonion water with Al

powder was used as the medium, and the voltage was 120 V. The results showed that the microhardness of the strengthening layer increased as I_p increased to 14 A. When the pulse width is 30 to 50 seconds, this layer's optimal microstructure and mechanical properties are attained. When the pulse interval surpasses 150 seconds, it impacts its usability [10]. I have studied the effect of different tool electrode materials, such as copper, copper-tungsten, and graphite, on processing efficiency during the machining of Inconel 718 using an electrical discharge process with a mixed dielectric liquid. The effect of these electrodes on the TWR, MRR, and WR was studied. The results showed that the highest MRR was 120.784 mg/min for copper electrode, followed by graphite electrode, which reduced to 46.88 mg/min, and the lowest MRR was for copper-tungsten with 17.029 mg/min. The surface roughness with 5.25 µm was achieved when a copper electrode was used. As for electrode corrosion and TWR, it was minimal when using a graphite electrode, which increased from 0.122 to 0.341% compared with that for copper electrode, which increased from 5.2 to 40.67%, and that for copper-tungsten, which increased from 7.5 to 18.34%. Copper electrodes suffer from disadvantages related to brittleness and difficulty in manufacturing. From an economic standpoint, the copper electrode is considered the best, in addition to it producing a high material removal rate and low surface roughness [11]. Investigated the effect of key parameters such as pulse current, pulse time, pulse on time, and pulse off time of EDM with GSP-70 grade graphite electrodes on AISI 304 stainless steel machining. The results showed that the factors most influencing the machining surface roughness of the AISI 304 stainless steel are pulse current, pulse on time, and pulse off time, where the best values for these parameters were pulse current (I_A) of 1.25 A, pulse on time (T_{on}) of 10 ps and pulse off time (T_{off}) of 3 ps, to obtain the lowest values of surface roughness [12]. Studied the machining of stainless steel specimens by experimenting with several materials such as copper (Cu), tungsten (W), and copper tungsten (Cu-W), and also varied the machining process parameters such as gap voltage and pulse on time. Through experimental results, the copper tool exhibited a notable improvement in electrical discharge efficiency and demonstrated significant tool wear. As a result of the high anodic wear occurring at low levels of gap voltage and T_{on}, the surface exhibits fewer surface imperfections. When these parameters are high, the process of high electrical discharge efficiency occurs, leading to a great number of surface imperfections. Meanwhile, the tungsten electrode exhibits lower electrode wear and electrical discharge efficiency. Therefore, in conditions of low operating parameters, the reduced tool wear results in an increased quantity of spark being exposed to the work surface and forming a greater number of surface imperfections. The lower discharge efficiency becomes more pronounced at higher operating conditions, resulting in less surface erosion [13]. Studied the machining of AISI 304 stainless steel in three dimensions (3D) by electric discharge machining (EDM) with a computer-aided design and manufacturing (CAD/CAM) system. The proposed approach included incorporating the electrode tool wear control technology into the CAD/CAM system. As per the claim, the proposed technique led to improved machining efficiency by around 30%, a reduction in the tool wear ratio from 0.04 to 0.02, an MRR increase from 15000 $\mu m^3/s$ to 25000 $\mu m^3/s$, and R_a reduced from 400 nm to 200 nm compared with conventional EDM [14]. Examined the impact of a modified pulse energy generation system on several performance measures. The experimental findings indicated that the iso-energetic pulse generator yields a reduced and uniformly distributed white layer thickness on the machined workpiece. This outcome is attributed to its ability to generate low-energy pulses with a very uniform distribution of energy. The analysis explicitly determined that peak current is critical in creating a white layer during the EDM process. In EDM, performance indicators are primarily determined by the energy discharged during machining. Stainless steel is appropriate for EDM when a dielectric medium is utilized because of its enhanced strength [15]. Used Taguchi experimental design to generate an L9 orthogonal matrix with the help of Minitab software to study the influencing parameters on machining 310L stainless steel during the process using an electrode tool made of copper to obtain output values in terms of MRR, TWR, and R_s. The results showed that the optimal values of (MRR = 20.83 mg/min), (TWR = 17.92 mg/min), and (R_s = 0.443 µm) at the current value of 20 A and pulse on time equal to 60 µs. SEM images confirmed these results [16]. Micro-EDM replaced the traditional EDM and then used micro-EDM of negative polarity to obtain a thin forming layer for machined 304 stainless steel. A copper electrode was used, and the operating parameters were set as follows: voltage of 250 V, pulse width of 7 µs, and a pulse interval of 5 µs. The results showed the presence of micro-cracks in the traditional EDM technique. When the surface was exposed to micro EDM and micro EDM with negative polarity at a voltage of 110 V, a pulse width of 0.5 microseconds, and a pulse interval of 15 microseconds, the quality of the surface improved, and the micro-cracks disappeared [17]. Examined the feasibility of using micro-EDM to quickly produce small metallic bipolar plates with a three-pass serpentine topology. The rib and channel dimensions were configured to be 500 µm in width, with a channel depth of 600 µm (resulting in an aspect ratio of 1.2), all contained inside a reaction area of 20 mm × 20 mm. The approach exhibited a remarkable material removal rate, reaching 7.2 $mm^3\ min^{-1}$. Nevertheless, the increased material-removal rate was shown to be associated with a corresponding rise in surface roughness inside the flow channels. The highest power densities achieved in single-cell experiments were 674 mW cm^{-2} and 647 mW cm^{-2} for flow channels with surface roughness of 0.715 µm Ra and 0.994 µm Ra, respectively. Although increasing surface roughness negatively influences cell performance, the research concluded that this effect was not statistically significant [18]. Titanium powder was added to the dielectric solution in different concentrations (5, 10, 15, and 20 g/l)

to study the effect of these additions on the quality of the resulting surface, especially at the MRR and R_s. In this study, the values of the operating process, such as Ip, V, and T_{on}, were kept constant. The results showed that the addition of powder led to an increase in the MRR with a reduction in surface roughness compared with the traditional EDM; the results also showed that a higher increase in the MRR with more reduction in R_s from 30 to 10 µm by increasing the powder rate [19]. The current study focuses on one of the most challenging materials, stainless steel 304L. If this material is machined using traditional procedures, the tool may be damaged, and the workpiece may suffer internal stress. Electrical discharge machining (EDM) is used to mill the stainless steel 304L to address this issue. This study aims to achieve a lower white layer thickness, lower heat-affected zone, and minimum surface crack density by improving input process parameters. In this experiment, a copper wire electrode was used. According to the experimental results, adding Al_2O_3-SiO_2 nano powder in dielectric decreases the white layer thickness of the machined surface. HAZ has dramatically improved; however, SCD has declined.

METHODOLOGY OF RESEARCH

The stainless steel 304L is used as a workpiece in this project. Nanoparticles are made from aluminum oxide (Al_2O_3) and silicon dioxide (SiO_2). Using a 1-5 g/l concentration and a mix fraction of 30-70% Al_2O_3 with SiO_2 balanced to integrate with kerosene dielectric. Figure 1 shows the workpiece dimensions (25.4 mm diameter x 5 mm thickness).

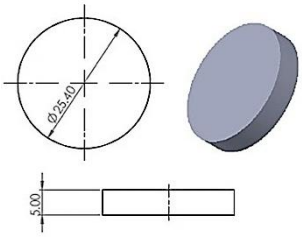

Fig. 1 Workpiece before machining (25.4 mm diameter x 5mm Thickness)

The machining properties of stainless steel 304L are investigated utilizing the electric discharge machining (EDM) process. As shown in Figure 2, the current study's tests are carried out on a numerically controlled electric discharge machine with the model number (CM 323+50N (CHAMBER EDM)).

Fig. 2 Electric discharge machine

Kerosene is utilized as a dielectric fluid. Figure 3 shows how the tests are carried out using a cylindrical copper electrode with a diameter of 16 mm and a length of 40 mm.

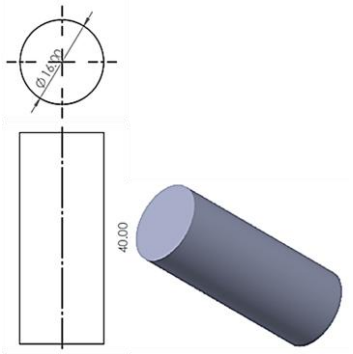

Fig. 3 Copper electrode (16 mm diameter x 40 mm length)

Table 1 contains complete measurements and thermophysical properties of the selected electrode.

Table 1
Specifications and thermo physical properties of the copper electrode

Diameter of tool (mm)	16
Tool length (mm)	40
Specific heat capacity (J/kg-ºC)	385
Thermal conductivity (W/m-ºC)	385
Thermal diffusivity (m^2/s)	1.11×10^{-4}
Density (Kg/m^3)	8960
Melting point (ºC)	1085
Thermal expansion coefficient at 20ºC (/ºC)	16.5×10^{-6}

Table 2 shows the chemical composition of the workpiece stainless steel 304L and the electrode characteristics and workpiece composition tested by the Ministry of Oil and Midland Refineries Company.

Table 2
Chemical composition of stainless steel 304L

Chemical element	Cr	Ni	Mn	Cu	Si	P	Ni	C	S	Fe
% composition	18.37	8.19	1.8	0.58	0.54	0.039	0.037	0.021	0.019	Balance

This experiment mixed 20-nm aluminum oxide particles and 50-nm silicon dioxide with a kerosene dielectric. Table 3 shows some of the critical and practical nano powder specifications used in the NPMEDM process, as tested at the University of Technology/Nano Center.

Table 3
The effective physical properties of nanoparticles in NPMEDM

Nanoparticles	Density (g/cm^3)	Thermal Conductivity (W/cmK)	Electrical Resistivity (µΩ.cm)	Particle size (nm)

Al_2O_3	3.89	1.5-2	10^3	20
SiO_2	2.4	1.3	10^8-10^{12}	50

Machining experiments using the response surface methodology (RSM) are conducted using the Design Expert 11. The study's input parameters include the electric discharge current, particle concentration, pulse on/off period, and nanoparticle mixing percentage. There are five stages of testing for each parameter. Table 4 contains a list of parameters and their respective ranges.

Table 4

Parameters and their levels

		Levels				
No.	**Parameters**	**1**	**2**	**3**	**4**	**5**
1	Pulse off time (µs)	25	50	75	100	125
2	Pulse on time (µs)	50	100	150	200	250
3	Peak current (A)	20	25	30	35	40
4	Mix of powder (% Al_2O_3)	30	40	50	60	70
5	Concentration (g/l)	1	2	3	4	5

The material removal rate (g/min) and electrode wear rate (g/min) due to machining time are computed using Equations (1) and (2), respectively.

Response characteristics include surface roughness (Ra), electrode wear rate (EWR), and material removal rate (MRR). The weight loss method is used to compute the MRR and EWR. The SR is measured using the Mahr Marsuf PS1 roughness tester, which averages three measurements from the cutting surface in different directions. Additionally, aluminum oxide nano powder is used in studies as a basis for determining particle composition percentage. The EDM machine's low voltage mode is used for all experiments.

$$MRR = \frac{InitialWeightofwork - FinalWeightofwork}{MachiningTime} \quad (1)$$

$$EWR = \frac{InitialWeightofElectrode - FinalWeightofElectrode}{MachiningTime} \quad (2)$$

RESULTS AND DISCUSSIONS

Response Surface Methodology (RSM) is a statistical technique to tackle complex multiple-response industrial problems. Response results are examined using the response surface methodology. The experimental protocols were created using core composite design concepts. Fifty full factorial experiments were carried out using the design matrix RSM developed. Peak current (I_p), pulse-on time (P_{on}), pulse-off time (P_{off}), powder concentration, and mixing ratio of powder are the five input process factors that are investigated in this study. Each of these parameters was investigated at five different levels for testing. Measures including Heat Affected Zone (HAZ), Surface Crack Density (SCD), and White Layer (WLT) were carried out using the response surface methodology. In this discipline, "Design Experts 11" is a highly renowned statistical software used to assess the responses [19]. Fifty trials were conducted with identical input process settings and conditions for NPMEDM. The results were then discussed using measured material removal rate, electrode wear rate, and surface roughness values.

Regression Model

The relationship between the input variables and response characteristics of the machining process was determined and analyzed based on Regression analysis. A Non-linear equation represented the relation that connects the input parameters with the responses in the regression analysis. Depending on the experimental output values, RSM developed mathematical models, and the general 2nd-order model was developed and adopted in the present work. Equations (3), (4), and (5) shown below illustrate the mathematical models for the output required performance measures:

$$\begin{aligned}\mathbf{WL} = {} & 17.4876 + 4.841 \cdot \mathrm{A} + 1.634 \cdot \mathrm{B} + -0.8945 \cdot \mathrm{C} + \\ & -0.3045 \cdot \mathrm{D} + -0.1965 \cdot \mathrm{E} + -0.14125 \cdot \mathrm{AB} + \\ & -0.224375 \cdot \mathrm{AC} + 0.1225 \cdot \mathrm{AD} + 0.09125 \cdot \mathrm{AE} + \\ & 0.128125 \cdot \mathrm{BC} + 0.1225 \cdot \mathrm{BD} + 0.0775 \cdot \mathrm{BE} + \\ & -0.125625 \cdot \mathrm{CD} + -0.066875 \cdot \mathrm{CE} + -0.09125 \cdot \mathrm{DE} + \\ & -0.607 \cdot \mathrm{A}^2 + 0.1855 \cdot \mathrm{B}^2 + -0.117 \cdot \mathrm{C}^2 + 0.11425 \cdot \\ & \mathrm{D}^2 + 0.12175 \cdot \mathrm{E}^2\end{aligned} \quad (3)$$

$$\begin{aligned}\mathbf{HAZ} = {} & 18.6555 + 4.5735 \cdot \mathrm{A} + 1.582 \cdot \mathrm{B} + -0.8915 \cdot \\ & \mathrm{C} + -0.256 \cdot \mathrm{D} + -0.213 \cdot \mathrm{E} + 0.25625 \cdot \mathrm{AB} + \\ & -0.384375 \cdot \mathrm{AC} + 0.0725 \cdot \mathrm{AD} + 0.0325 \cdot \mathrm{AE} + 0.22 \cdot \\ & \mathrm{BC} + 0.243125 \cdot \mathrm{BD} + 0.111875 \cdot \mathrm{BE} + -0.085 \cdot \mathrm{CD} + \\ & 0.0775 \cdot \mathrm{CE} + -0.073125 \cdot \mathrm{DE} + -0.149375 \cdot \mathrm{A}^2 + \\ & 0.413125 \cdot \mathrm{B}^2 + -0.074375 \cdot \mathrm{C}^2 + 0.308125 \cdot \mathrm{D}^2 + \\ & 0.335625 \cdot \mathrm{E}^2\end{aligned} \quad (4)$$

$$\begin{aligned}\mathbf{SCD} = {} & 0.02536 + 0.0101 \cdot \mathrm{A} + 0.00345 \cdot \mathrm{B} + -0.0017 \cdot \\ & \mathrm{C} + -0.00065 \cdot \mathrm{D} + -0.00055 \cdot \mathrm{E} + -0.0005625 \cdot \mathrm{AB} + \\ & -6.25\mathrm{e}-05 \cdot \mathrm{AC} + 0.0004375 \cdot \mathrm{AD} + -6.69602\mathrm{e}-19 \cdot \\ & \mathrm{AE} + 0.000375 \cdot \mathrm{BC} + 0.0005 \cdot \mathrm{BD} + 6.25\mathrm{e}-05 \cdot \mathrm{BE} + \\ & -5.11892\mathrm{e}-19 \cdot \mathrm{CD} + -6.25\mathrm{e}-05 \cdot \mathrm{CE} + 6.25\mathrm{e}-05 \cdot \\ & \mathrm{DE} + -0.000825 \cdot \mathrm{A}^2 + 0.000925 \cdot \mathrm{B}^2 + 5\mathrm{e}-05 \cdot \mathrm{C}^2 + \\ & 0.000175 \cdot \mathrm{D}^2 + 0.0003 \cdot \mathrm{E}^2\end{aligned} \quad (5)$$

where:

A = Current,

B = Pulse on,

C = Pulse off,

D = Nano powder Concentration,

E = Nano powder Mixing Ratio Al_2O_3%-balanced SiO_2.

The predicted WLT, HAZ, and SCD values were determined by equations (3), (4), and (5). Based on the outputs, the precision of predicting the developed model appeared acceptable. Tables 5, 6, and 7 and Figures 4, 6, and 8 present the actual versus predicted values. The average probability plots for each mathematical model were performed as shown in the previous figures. Figures 5, 7, and 9 depict the average probability of the machining characteristics, which are utilized to check the normality assumption and the normal distribution of errors.

Table 5

Prediction Accuracy of WLT for NPMEDM process

Run	I_p	P_{on} (µs)	P_{off} (µs)	Con. (g/L)	Mix of Al_2O_3%-balanced SiO_2	Exp. WLT (µm)	Pred. WLT (µm)	Error Exp./Pred.
1	30	250	75	3	50	21.35	21.50	0.993
2	35	100	50	4	40	21.68	21.81	0.994
3	30	150	75	5	50	17.17	17.34	0.990
4	35	100	100	2	40	19.90	19.87	1.001
5	30	150	75	3	50	17.50	17.49	1.001
6	25	200	100	2	60	13.76	13.82	0.996
7	35	100	100	4	60	19.17	18.52	1.035
8	35	200	50	2	40	24.90	24.31	1.024
9	30	150	75	3	50	19.90	17.49	1.138
10	40	150	75	3	50	24.12	24.74	0.975
11	30	50	75	3	50	14.80	14.96	0.989
12	35	200	100	4	40	22.37	22.53	0.993
13	30	150	75	3	30	18.32	18.37	0.997
14	30	150	75	3	50	16.75	17.49	0.958
15	25	100	50	4	60	10.80	10.55	1.023
16	30	150	25	3	50	18.82	18.81	1.001
17	30	150	125	3	50	14.91	15.23	0.979
18	35	200	100	2	40	22.81	22.72	1.004
19	35	100	50	4	60	21.47	21.39	1.004
20	30	150	75	3	50	17.75	17.49	1.015
21	30	150	75	3	50	16.89	17.49	0.966
22	35	100	50	2	60	21.76	21.93	0.992
23	25	100	50	4	40	11.54	11.33	1.018
24	35	200	100	2	60	22.59	22.71	0.995
25	30	150	75	1	50	18.41	18.55	0.992
26	35	200	50	2	60	24.82	24.57	1.010
27	25	200	100	4	60	13.34	12.78	1.044
28	25	100	50	2	60	11.69	11.58	1.009
29	35	200	100	4	60	22.19	22.16	1.001
30	35	100	50	2	40	21.90	21.98	0.996
31	30	150	75	3	50	16.69	17.49	0.954
32	25	100	100	4	60	7.43	7.57	0.982
33	25	100	100	4	40	9.81	9.62	1.020
34	25	100	100	2	40	10.66	10.79	0.988
35	25	200	50	4	40	14.36	14.72	0.976
36	35	100	100	2	60	19.75	19.56	1.010
37	20	150	75	3	50	5.69	5.38	1.058
38	35	200	50	4	40	24.74	24.63	1.005
39	35	200	50	4	60	24.50	24.52	0.999
40	25	100	100	2	60	10.57	10.10	1.046
41	30	150	75	3	50	16.64	17.49	0.952
42	30	150	75	3	50	18.09	17.49	1.034
43	35	100	100	4	40	19.42	19.20	1.012
44	25	200	50	2	60	14.54	14.79	0.983
45	25	200	50	4	60	14.27	14.25	1.002
46	25	200	100	2	40	14.19	14.19	1.000
47	30	150	75	3	70	17.32	17.58	0.985
48	25	200	50	2	40	14.69	14.89	0.986
49	25	100	50	2	40	11.90	12.00	0.992
50	25	200	100	4	40	13.64	13.52	1.009

Table 6

Prediction Accuracy of HAZ for NPMEDM process

Run	I_p (A)	P_{on} (µs)	P_{off} (µs)	Con. (g/L)	Mix of Al_2O_3%-balanced SiO_2	Exp. HAZ (µm)	Pred. HAZ (µm)	Error Exp./Pred.
1	30	250	75	3	50	23.88	23.47	1.017
2	35	100	50	4	40	24.19	23.82	1.015
3	30	150	75	5	50	18.80	19.38	0.970
4	35	100	100	2	40	21.97	21.38	1.028
5	30	150	75	3	50	18.57	18.66	0.995
6	25	200	100	2	60	15.61	16.14	0.967
7	35	100	100	4	60	20.82	19.93	1.045
8	35	200	50	2	40	27.31	26.88	1.016
9	30	150	75	3	50	18.62	18.66	0.998
10	40	150	75	3	50	24.98	27.21	0.918
11	30	50	75	3	50	16.43	17.14	0.958
12	35	200	100	4	40	24.51	24.88	0.985
13	30	150	75	3	30	20.77	20.42	1.017
14	30	150	75	3	50	18.33	18.66	0.983
15	25	100	50	4	60	13.17	13.32	0.989
16	30	150	25	3	50	20.09	20.14	0.997
17	30	150	125	3	50	16.32	16.58	0.985
18	35	200	100	2	40	25.03	24.79	1.010
19	35	100	50	4	60	23.43	22.94	1.022
20	30	150	75	3	50	19.08	18.66	1.023
21	30	150	75	3	50	18.91	18.66	1.014
22	35	100	50	2	60	24.17	23.76	1.017
23	25	100	50	4	40	14.34	14.34	1.000
24	35	200	100	2	60	25.13	24.95	1.007
25	30	150	75	1	50	20.67	20.40	1.013
26	35	200	50	2	60	26.87	26.74	1.005
27	25	200	100	4	60	15.70	15.65	1.003
28	25	100	50	2	60	14.44	14.44	1.000
29	35	200	100	4	60	25.35	24.75	1.024
30	35	100	50	2	40	24.19	24.36	0.993
31	30	150	75	3	50	18.21	18.66	0.976
32	25	100	100	4	60	11.51	11.65	0.988
33	25	100	100	4	40	12.38	12.56	0.986
34	25	100	100	2	40	13.46	13.73	0.981
35	25	200	50	4	40	16.44	16.81	0.978
36	35	100	100	2	60	21.25	21.10	1.007
37	20	150	75	3	50	10.83	8.91	1.215
38	35	200	50	4	40	27.91	27.32	1.022
39	35	200	50	4	60	26.91	26.88	1.001
40	25	100	100	2	60	13.23	13.31	0.994
41	30	150	75	3	50	18.72	18.66	1.003
42	30	150	75	3	50	19.11	18.66	1.024
43	35	100	100	4	40	20.71	20.50	1.010
44	25	200	50	2	60	16.52	16.39	1.008
45	25	200	50	4	60	15.91	16.24	0.979
46	25	200	100	2	40	15.81	16.11	0.982
47	30	150	75	3	70	18.92	19.57	0.967
48	25	200	50	2	40	15.71	16.67	0.943
49	25	100	50	2	40	14.98	15.16	0.988
50	25	200	100	4	40	15.90	15.91	0.999

Table 7
Prediction Accuracy of SCD for NPMEDM process

Run	I_p (A)	P_{on} (µs)	P_{off} (µs)	Con. (g/L)	Mix of Al_2O_3%-balanced SiO_2	Exp. SCD (µm/µm²)	Pred. SCD (µm/µm²)	Error Exp./Pred.
1	30	250	75	3	50	0.0360	0.0360	1.0011
2	35	100	50	4	40	0.0350	0.0351	0.9969
3	30	150	75	5	50	0.0230	0.0248	0.9289
4	35	100	100	2	40	0.0330	0.0325	1.0151
5	30	150	75	3	50	0.0250	0.0254	0.9858
6	25	200	100	2	60	0.0190	0.0186	1.0210
7	35	100	100	4	60	0.0310	0.0297	1.0425
8	35	200	50	2	40	0.0410	0.0406	1.0108
9	30	150	75	3	50	0.0250	0.0254	0.9858
10	40	150	75	3	50	0.0390	0.0423	0.9229
11	30	50	75	3	50	0.0210	0.0222	0.9477
12	35	200	100	4	40	0.0380	0.0384	0.9906
13	30	150	75	3	30	0.0290	0.0277	1.0484
14	30	150	75	3	50	0.0270	0.0254	1.0647
15	25	100	50	4	60	0.0120	0.0118	1.0161
16	30	150	25	3	50	0.0290	0.0290	1.0014
17	30	150	125	3	50	0.0210	0.0222	0.9477
18	35	200	100	2	40	0.0380	0.0379	1.0024
19	35	100	50	4	60	0.0350	0.0341	1.0253
20	30	150	75	3	50	0.0260	0.0254	1.0252
21	30	150	75	3	50	0.0250	0.0254	0.9858
22	35	100	50	2	60	0.0360	0.0354	1.0159
23	25	100	50	4	40	0.0130	0.0128	1.0168
24	35	200	100	2	60	0.0370	0.0367	1.0086
25	30	150	75	1	50	0.0280	0.0274	1.0234
26	35	200	50	2	60	0.0400	0.0396	1.0105
27	25	200	100	4	60	0.0180	0.0176	1.0251
28	25	100	50	2	60	0.0150	0.0149	1.0094
29	35	200	100	4	60	0.0380	0.0374	1.0165
30	35	100	50	2	40	0.0360	0.0367	0.9820
31	30	150	75	3	50	0.0260	0.0254	1.0252
32	25	100	100	4	60	0.0080	0.0077	1.0444
33	25	100	100	4	40	0.0080	0.0089	0.9004
34	25	100	100	2	40	0.0120	0.0122	0.9848
35	25	200	50	4	40	0.0200	0.0209	0.9553
36	35	100	100	2	60	0.0320	0.0310	1.0311
37	20	150	75	3	50	0.0040	0.0039	1.0256
38	35	200	50	4	40	0.0420	0.0410	1.0241
39	35	200	50	4	60	0.0410	0.0403	1.0177
40	25	100	100	2	60	0.0100	0.0107	0.9337
41	30	150	75	3	50	0.0260	0.0254	1.0252
42	30	150	75	3	50	0.0240	0.0254	0.9464
43	35	100	100	4	40	0.0320	0.0310	1.0336
44	25	200	50	2	60	0.0210	0.0213	0.9878
45	25	200	50	4	60	0.0200	0.0202	0.9896
46	25	200	100	2	40	0.0190	0.0198	0.9579
47	30	150	75	3	70	0.0230	0.0255	0.9034
48	25	200	50	2	40	0.0210	0.0222	0.9445
49	25	100	50	2	40	0.0160	0.0161	0.9947
50	25	200	100	4	40	0.0190	0.0185	1.0251

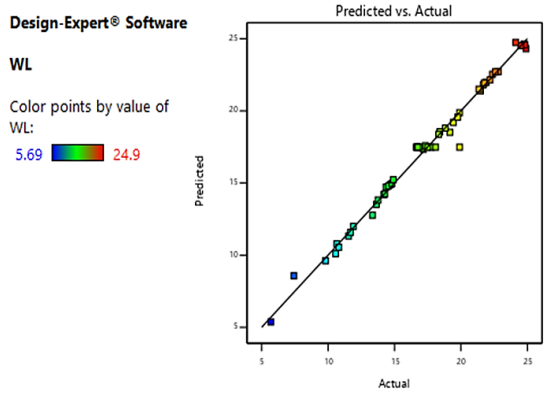

Fig. 4 Predicted vs. Actual (Experiment) WLT

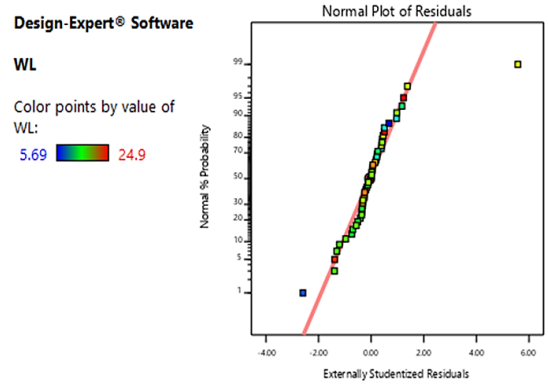

Fig. 5 Normal vs. Externally Studentized Residuals WLT

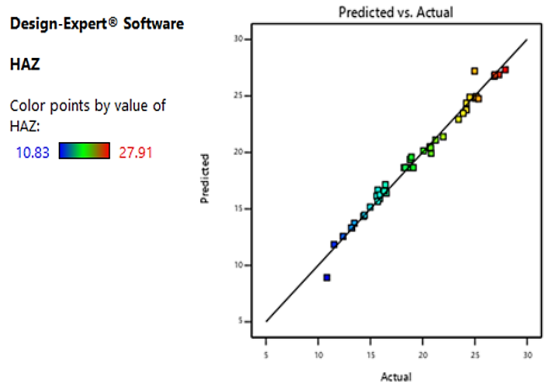

Fig. 6 Predicted vs. Actual (Experiment) HAZ

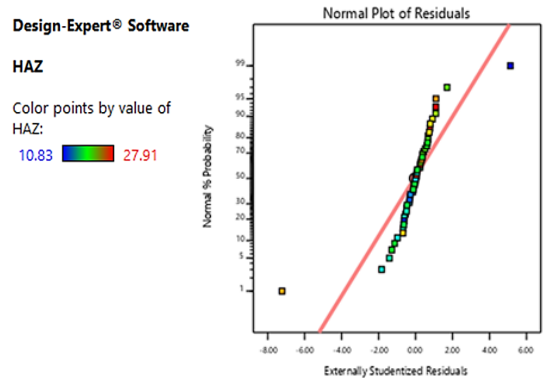

Fig. 7 Normal vs. Externally Studentized Residuals HAZ

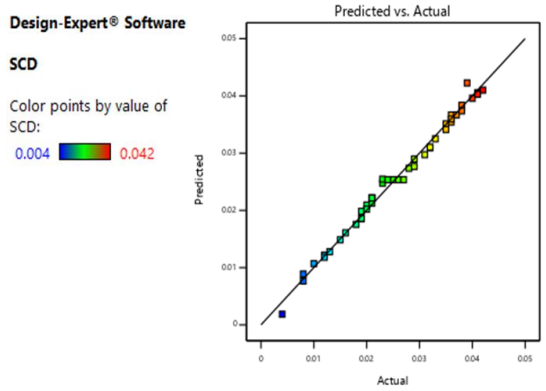

Fig. 8 Predicted vs. Actual (Experiment) SCD

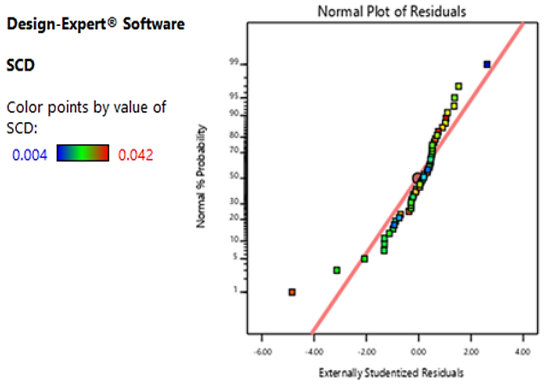

Fig. 9 Normal vs. Externally Studentized Residuals SCD

Statistical Analysis for the NPMEDM Process

The goodness of the second-order model and the evaluation of the dominant parameters of all output characteristics of the machining process were implemented according to (ANOVA) technique. ANOVA is used to test the resulting readings' hypotheses at a confidence level of (95)%. Fisher statistical test (F-test) was adopted to determine the significance of the parameters. The maximum levels of the (F-test) indicate the more influential parameter, and the p-value for the F-statistical represents the probability of output measured data.

If the p-value ≤ 0.05, the parameter has a statistically impressive influence. The contribution percentage of individual parameters can be determined from the ANOVA table using the following expression [20]:

$$Percentage\ contribution\ (C\%) = \frac{Sum\ of\ Square\ of\ Variation}{Total\ Sum\ of\ Square\ of\ Variation} \cdot 100 \quad (6)$$

Table 8
ANOVA for WLT Response

Source	Sum of Squares	df	Mean Square	F-value	p-value
Model	1100.80	20	55.04	127.02	< 0.0001
A-Current	937.41	1	937.41	2163.29	< 0.0001
B-Pulse on	106.80	1	106.80	246.46	< 0.0001
C-Pules off	32.01	1	32.01	73.86	< 0.0001
D-Concentration	3.71	1	3.71	8.56	0.0066
E-Mix of Al%-Si	1.54	1	1.54	3.56	0.0691
AB	0.6384	1	0.6384	1.47	0.2346
AC	1.61	1	1.61	3.72	0.0637
AD	0.4802	1	0.4802	1.11	0.3012
AE	0.2665	1	0.2665	0.6149	0.4393
BC	0.5253	1	0.5253	1.21	0.2799
BD	0.4802	1	0.4802	1.11	0.3012
BE	0.1922	1	0.1922	0.4435	0.5107
CD	0.5050	1	0.5050	1.17	0.2892
CE	0.1431	1	0.1431	0.3303	0.5699
DE	0.2665	1	0.2665	0.6149	0.4393
A^2	11.79	1	11.79	27.21	< 0.0001
B^2	1.10	1	1.10	2.54	0.1218
C^2	0.4380	1	0.4380	1.01	0.3230
D^2	0.4177	1	0.4177	0.9639	0.3343
E^2	0.4743	1	0.4743	1.09	0.3041
Residual	12.57	29	0.4333		
Lack of Fit	4.07	22	0.1850	0.1525	0.9997
Pure Error	8.50	7	1.21		
Cor Total	1113.36	49			

Table 9
ANOVA for HAZ Response

Source	Sum of Squares	df	Mean Square	F-value	p-value
Model	997.47	20	49.87	91.29	< 0.0001
A-Current	836.68	1	836.68	1531.41	< 0.0001
B-Pulse on	100.11	1	100.11	183.23	< 0.0001
C-Pules off	31.79	1	31.79	58.19	< 0.0001
D-Concentration	2.62	1	2.62	4.80	0.0367
E-Mix of Al%-Si	1.81	1	1.81	3.32	0.0787
AB	2.10	1	2.10	3.85	0.0595
AC	4.73	1	4.73	8.65	0.0064
AD	0.1682	1	0.1682	0.3079	0.5832
AE	0.0338	1	0.0338	0.0619	0.8053
BC	1.55	1	1.55	2.83	0.1030
BD	1.89	1	1.89	3.46	0.0730
BE	0.4005	1	0.4005	0.7331	0.3989
CD	0.2312	1	0.2312	0.4232	0.5205
CE	0.1922	1	0.1922	0.3518	0.5577
DE	0.1711	1	0.1711	0.3132	0.5800
A^2	0.7140	1	0.7140	1.31	0.2623
B^2	5.46	1	5.46	10.00	0.0037
C^2	0.1770	1	0.1770	0.3240	0.5736
D^2	3.04	1	3.04	5.56	0.0253
E^2	3.60	1	3.60	6.60	0.0156
Residual	15.84	29	0.5463		
Lack of Fit	15.09	22	0.6858	6.34	0.0090
Pure Error	0.7570	7	0.1081		
Cor Total	1013.32	49			

Table 10
ANOVA for SCD Response

Source	Sum of Squares	df	Mean Square	F-value	p-value
Model	0.0048	20	0.0002	142.80	< 0.0001
A-Current	0.0041	1	0.0041	2436.31	< 0.0001
B-Pulse on	0.0005	1	0.0005	284.27	< 0.0001
C-Pules off	0.0001	1	0.0001	69.02	< 0.0001
D-Concentration	0.0000	1	0.0000	10.09	0.0035
E-Mix of Al%-Si	0.0000	1	0.0000	7.22	0.0118
AB	0.0000	1	0.0000	6.05	0.0202
AC	1.250E-07	1	1.250E-07	0.0746	0.7866
AD	6.125E-06	1	6.125E-06	3.66	0.0658
AE	0.0000	1	0.0000	0.0000	1.0000
BC	4.500E-06	1	4.500E-06	2.69	0.1120
BD	8.000E-06	1	8.000E-06	4.78	0.0371
BE	1.250E-07	1	1.250E-07	0.0746	0.7866
CD	0.0000	1	0.0000	0.0000	1.0000
CE	1.250E-07	1	1.250E-07	0.0746	0.7866
DE	1.250E-07	1	1.250E-07	0.0746	0.7866
A^2	0.0000	1	0.0000	13.00	0.0012
B^2	0.0000	1	0.0000	16.35	0.0004
C^2	8.000E-08	1	8.000E-08	0.0478	0.8285
D^2	9.800E-07	1	9.800E-07	0.5851	0.4505
E^2	2.880E-06	1	2.880E-06	1.72	0.2000
Residual	0.0000	29	1.675E-06		
Lack of Fit	0.0000	22	1.935E-06	2.26	0.1357
Pure Error	6.000E-06	7	8.571E-07		
Cor Total	0.0048	49			

The mean Square value can be estimated by dividing the Sum of the Square value of each output characteristic by df. At the same time, the F-value was found by dividing the ratio of the Mean Square of the terms by the Mean Square of the residual. Figures 10, 11, and 12 reveal the percentage contribution of parameters. Figure 10 shows that the most influential parameter that affects (WLT) is current, with a percentage contribution of (84.196)%, and the percentages of the rest of the parameters were (9.592)% and (2.875)% for pulse on and pulse off, respectively.

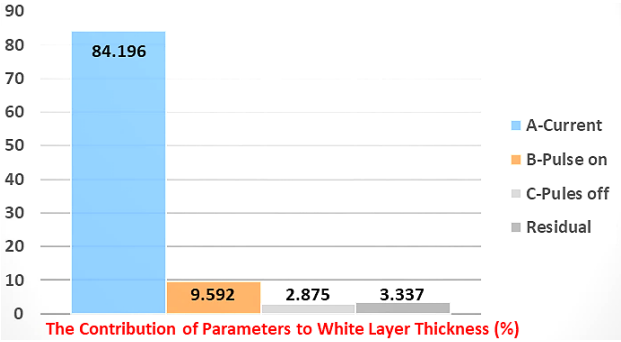

Fig. 10 The Percentage Contribution of Parameters to WLT

Figure 11 shows that it can be concluded the most influential factor that affects the HAZ is current, with a percentage contribution of (82.568)%. In contrast, the percentages of other factors are (9.879)% and (3.137)% for pulse on and pulse off, respectively.

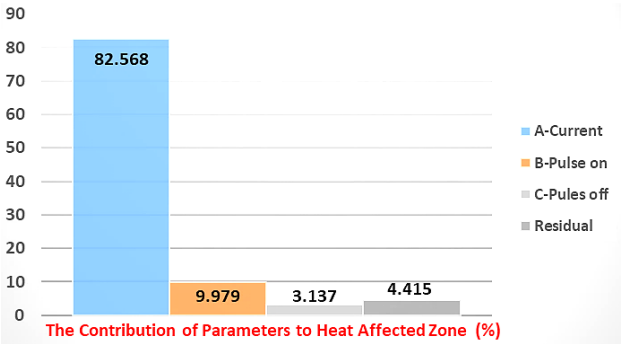

Fig. 11 The Percentage Contribution of Parameters to HAZ

Finally, in Figure 12 for SCD response, it can be noted that the highest participation for current is (84.445)%, and the involvement of other parameters is (9.853)% and (2.392)% for pulse on and pulse off, respectively.

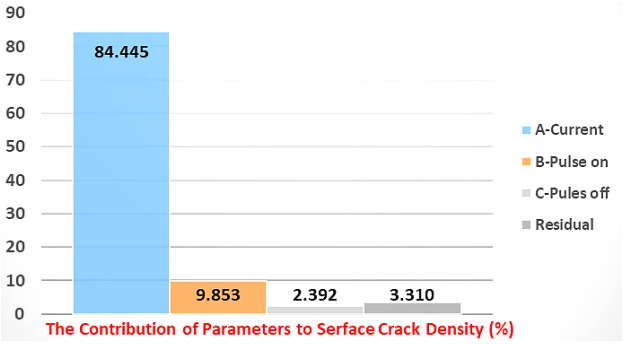

Fig. 12 The Percentage Contribution of Parameters to SCD

The **Model F-value** of 127.02 implies the model is significant. There is only a 0.01% chance that an F-value this large could occur due to noise. **P-values** less than 0.0500 indicate model terms are important. A, B, C, D, and A^2 are considerable model terms. Values greater than 0.1000 indicate the model terms are not significant. If there are many insignificant model terms (not counting those required to support hierarchy), model reduction may improve your model. The **Lack of Fit F-value** of 0.15 implies that the Lack of Fit is insignificant relative to the pure error. There is a 99.97% chance that a Lack of Fit F-value this large could occur due to noise. A non-significant lack of fit is good – the model must be fit.

The **Model F-value** of 91.29 implies the model is significant. There is only a 0.01% chance that an F-value this large could occur due to noise. **P-values** less than 0.0500 indicate model terms are significant. In this case A, B, C, D, AC, B^2, D^2, E^2 are significant model terms. Values greater than 0.1000 indicate the model terms are not significant. If there are many insignificant model terms (not counting those required to support hierarchy), model reduction may improve your model. The **Lack of Fit F-value** of 6.34 implies the Lack of Fit is significant. There is only a 0.90% chance that a Lack of Fit F-value this large could occur due to noise. Significant lack of fit is bad – the model needs to be fit.

The **Model F-value** of 142.80 implies the model is significant. There is only a 0.01% chance that an F-value this large could occur due to noise. **P-values** less than 0.0500 indicate model terms are important. In this case, A, B, C, D, E, AB, BD, A^2, and B^2 are significant model terms. Values greater than 0.1000 indicate the model terms are not significant. If there are many insignificant model terms (not counting those required to support hierarchy), model reduction may improve your model. The **Lack of Fit F-value** of 2.26 implies the Lack of Fit is insignificant relative to the pure error. There is a 13.57% chance that a Lack of Fit F-value this large could occur due to noise. A non-significant lack of fit is good – the model needs to be fit.

Parametric Analysis of WLT

In Figure 13, a 3D contour diagram illustrating the impacts of nano powder concentration and nano powder mixing ratio on WLT is produced using response surface methodology (RSM) while preserving the default values of I_p, P_{on}, and P_{off}, which are (35 Amp.), (200 µs), and (50 µs), respectively.

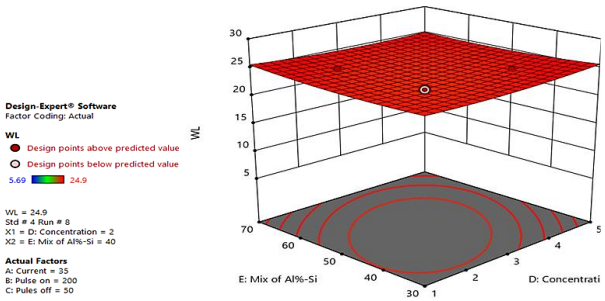

Fig. 13 Contour diagram of Max WLT vs. Con. and Mix%

The max WLT is demonstrated to fluctuate with nano powder concentration (2 g/L) and nano powder mixing ratio up to 40% by the relationship between nano powder concentration and nano powder mixing ratio. This finding supports the idea that, for a given concentration (2 g/L), a continual increase in WLT can be anticipated. The observed increase in (WLT) with increasing Al_2O_3 mixing ratio is often attributed to the increased expulsion energy available during this process. The increased discharge energy caused by nanoparticles promotes the melting and vaporization of materials and tool materials above the machining region.

A three-dimensional contour map, shown in Figure 14, illustrates the low White Layer Thickness (WLT) that may be achieved by increasing the Al_2O_3 mixing ratio to 50% and concentration to (3 g/L) while keeping the I_p (20 A), P_{on} (150 µs), and P_{off} (75 µs) constant.

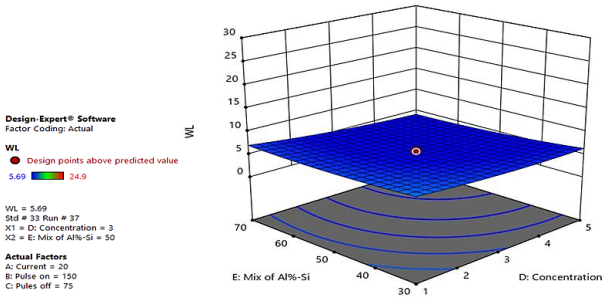

Fig. 14 Contour diagram of Min WLT vs. Pulse-on and current

This low EWR value can be explained by pointing out that the amount of melted and evaporated electrode material likewise falls with a drop in the discharge energy transferred (by nanoparticles).

It can be elucidated with the phenomenon that a maximum time of P_{off} allows to clean the debris and flush away the melted material from the machining region, due to that minimum recast layer thickness is produced.

Parametric Analysis of HAZ

Response surface methodology (RSM) is used in Figure 15 to create a 3D contour diagram that shows the effects of nano powder concentration and nano powder mixing ratio on HAZ while maintaining the default values of I_p, P_{on}, and P_{off}, which are (35 A), (200 µs), and (50 µs), respectively.

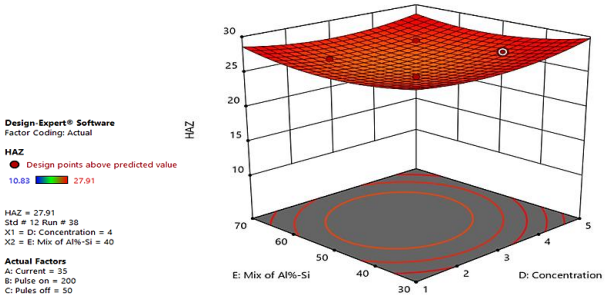

Fig. 15 Contour diagram of HAZ MRR vs. Con. and Mix%

The link between nano powder concentration and nano powder mixing ratio shows that the maximum HAZ varies with nano powder concentration (4 g/L) and nano powder mixing ratio up to 40%. This result confirms the hypothesis that a steady rise in HAZ can be expected for a certain concentration (4 g/L). The higher expulsion energy available during this process is generally attributed to the observed increase in (HAZ) with increasing Al_2O_3 mixing ratio because of the higher energy of discharge. The increased discharge energy caused by nanoparticles promotes the melting and vaporization of materials and tool materials above the machining region.

The low Heat Affected Zone (HAZ) can be attained by raising the Al_2O_3 mixing ratio to 50% and concentration decrease to 3 g/L while maintaining the I_p (20 A), P_{on} (150 µs), and P_{off} (75 µs) depicted in a three-dimensional contour map in Figure 16.

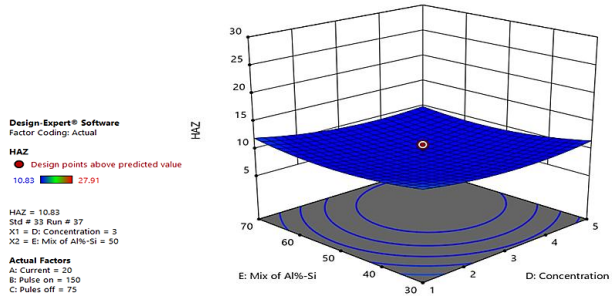

Fig. 16 Contour diagram of Min HAZ vs. Pulse-on and current

The fact that more melted and evaporated electrode material also decreases as discharge energy delivered (via nanoparticles) decreases helps to explain this low EWR value.

The phenomena that, at a maximum time of P_{off}, permits the removal of debris and melted material from the machining region can be used to explain it. As a result, the minimum thickness of the heat-affected zone and the minimum thickness of the recast layer are generated.

Parametric Analysis of SCD

This depends on the fact that the thermal stresses created on the machined zone caused the fractures to emerge, which started at the top surface of the recast layer and spread to the HAZ. Therefore, when the pulse duration is maximized, a significant amount of heat is transferred to the machined surface, causing thermal stresses to form

that surpass the material's greater strength and, as a result, maximizing the density of surface cracks.

Figure 17 shows that the maximum SCD fluctuates with nano powder concentration (4 g/L) and nano powder mixing ratio up to 40%, according to the relationship between the two parameters while maintaining the default values of I_p, P_{on}, and P_{off}, which are (35 A), (200 µs), and (50 µs), respectively.

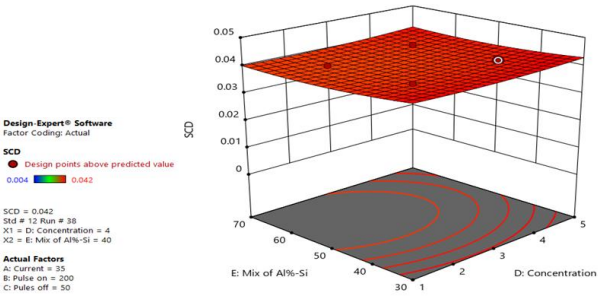

Fig. 17 Contour diagram of Max SCD vs. Con. and Mix%

This finding supports the theory that, at a given concentration (4 g/L), a continuous increase in SCD can be anticipated. The observed increase in SCD with an increased Al_2O_3 mixing ratio is often attributed to the higher expulsion energy available during this phase. Due to the discharge's increased energy and thermal stress. Because nanoparticles' enhanced discharge energy encourages the melting and evaporation of materials, including tool materials, above the machining region.

Figure 18 shows a three-dimensional contour map depicting the low Surface Crack Density (SCD) achieved by increasing the Al_2O_3 mixing ratio to 50% and decreasing the concentration to 3 g/L while retaining I_p (20 A), P_{on} (150 µs), and P_{off} (75 µs).

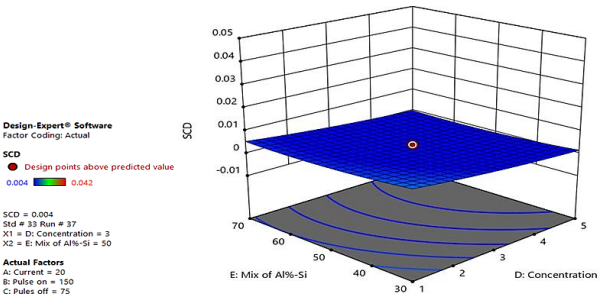

Fig. 18 Contour diagram of Min SCD vs. Pulse-on and current

The fact that more melted and evaporated electrode material is reduced when discharge energy given (by nanoparticles) lowers helps to explain the low EWR value.

CONCLUSION

The current work improves the output responses (surface topography) of EDM, such as WLT, HAZ, and SCD, for NPMEDM. Al_2O_3 and SiO_2 nanoparticles have electrical solid conductivity and physical qualities that decrease Kerosene breakdown strength and spark delay time. The white layer thickness is decreased when the nanoparticle concentration is mixed with the kerosene dielectric fluid. That makes the thermal conductivity of nanofluid much higher than that of conventional dielectric and increases the white layer thickness. It is found that WLT increases at larger discharge currents. Experimentally, we obtained an improvement in surface response, decreasing WLT, HAZ, and SCD by 5.8%, 17.7%, and 2.6%, respectively, using the Design Expert 11 program. Peak current is a significant factor for WLT, HAZ, and SCD at 84.2%, 82.6%, and 84.5%, respectively. The developed mathematical model for WLT, HAZ, and SCD within this work interval can effectively optimize the selection of the NPMEDM parameters to achieve good performance and surface integrity.

REFERENCES

[1] Shabgard, M.R. and Khosrozadeh, B., (2016). Comparative study of adding nano powders in dielectric effects on outputs and surface integrity of Ti-6Al-4V alloy in Electrical Discharge Machining. *Modares Mechanical Engineering*, *16*(2), pp. 41-50.

[2] Talla, G., Gangopadhyay, S. and Biswas, C.K., (2017). Influence of graphite powder mixed EDM on the surface integrity characteristics of Inconel 625. *Particulate Science and Technology*, *35*(2), pp. 219-226.

[3] Talla, G., Gangopadhyay, S. and Biswas, C.K., (2018). Effect of impregnated powder materials on surface integrity aspects of Inconel 625 during electrical discharge machining. *Proceedings of the Institution of Mechanical Engineers, Part B: Journal of Engineering Manufacture*, *232*(7), pp. 1259-1272.

[4] Singh, G., Sidhu, S.S., Bains, P.S. and Bhui, A.S., (2019). Surface evaluation of ED machined 316L stainless steel in TiO_2 nano-powder mixed dielectric medium. *Materials Today: Proceedings*, *18*, pp. 1297-1303.

[5] Sahu, D.R. and Mandal, A., (2020). Critical analysis of surface integrity parameters and dimensional accuracy in powder-mixed EDM. *Materials and Manufacturing Processes*, *35*(4), pp. 430-441.

[6] Taherkhani, A., Ilani, M.A., Ebrahimi, F., Huu, P.N., Long, B.T., Van Dong, P., Tam, N.C., Minh, N.D. and Van Duc, N., (2021). Investigation of surface quality in Cost of Goods Manufactured (COGM) method of µ-Al_2O_3 Powder-Mixed-EDM process on machining of Ti-6Al-4V. *The International Journal of Advanced Manufacturing Technology*, *116*(5), pp. 1783-1799.

[7] Furutania, K., Saneto, A., Takezawa, H., Mohri, N. and Miyake, H., (2001). Accretion of titanium carbide by electrical discharge machining with powder suspended in working fluid. *Precision Engineering*, *25*(2), pp. 138-144.

[8] Kumar, A., Maheshwari, S., Sharma, C. and Beri, N., 2012. Machining efficiency evaluation of cryogenically treated copper electrode in additive mixed EDM. *Materials and Manufacturing Processes*, *27*(10), pp. 1051-1058.

[9] Zain, Z.M., Ndaliman, M.B., Khan, A.A. and Ali, M.Y., (2014). Improving micro-hardness of stainless steel through powder-mixed electrical discharge machining. *Proceedings of the Institution of Mechanical Engineers, Part C: Journal of Mechanical Engineering Science*, *228*(18), pp. 3374-3380.

[10] Wang, J.L., Yang, H. and Li, M., (2014). Study on discharge parameters of surface strengthening with powder mixed near dry EDM for H13 steel. *Applied Mechanics and Materials*, *602*, pp. 757-760.

[11] Kuppan, P., Narayanan, S., Oyyaravelu, R. and Balan, A.S.S., (2017). Performance evaluation of electrode materials in

electric discharge deep hole drilling of Inconel 718 superalloy. *Procedia engineering*, *174*, pp. 53-59.

[12] Hernández-Castillo, I., Sánchez-López, O., Lancho-Romero, G.A. and Castañeda-Roldán, C.H., (2018). An experimental study of surface roughness in electrical discharge machining of AISI 304 stainless steel. *Ingeniería e Investigación*, *38*(2), pp. 90-96.

[13] Jithin, S., Shetye, S.S., Rodrigues, J.J., Mhetre, K.S., Mastud, S.A. and Joshi, S.S., (2018). Analysis of electrical discharge texturing using different electrode materials. *Advances in Materials and Processing Technologies*, *4*(3), pp. 466-479.

[14] Li, J.Z., Xiao, L., Wang, H., Yu, H.L. and Yu, Z.Y., (2013). Tool wear compensation in 3D micro EDM based on the scanned area. *Precision Engineering*, *37*(3), pp.753-757.

[15] Muthuramalingam, T., (2019). Measuring the influence of discharge energy on white layer thickness in electrical discharge machining process. *Measurement*, *131*, pp. 694-700.

[16] Singh, G., Bhui, A.S., Lamichhane, Y., Mukhiya, P., Kumar, P. and Thapa, B., (2019). Machining performance and influence of process parameters on stainless steel 316L using die-sinker EDM with Cu tool. *Materials Today: Proceedings*, *18*, pp. 2468-2476.

[17] Xu, B., Chen, S.G., Liang, X., Lei, J.G., Shi, H.Y., Fu, L.Y., Yang, J., Peng, T.J., Zhao, H. and Zhu, L.K., (2020). Recast layer removal of 304 stainless steel by combining micro-EDM with negative polarity micro-EDM. *The International Journal of Advanced Manufacturing Technology*, *107*, pp. 4713-4723.

[18] Razak, M.A., Abdul-Rani, A.M. and Nanimina, A.M., (2015). Improving EDM efficiency with silicon carbide powder-mixed dielectric fluid. *International Journal of Materials, Mechanics and Manufacturing*, *3*(1), pp. 40-43.

[19] Singh, B., Kumar, J. and Kumar, S., (2017). Optimization and surface modification in electrical discharge machining of AA 6061/SiCp composite using Cu-W electrode. *Proceedings of the Institution of Mechanical Engineers, Part L: Journal of Materials: Design and Applications*, *231*(3), pp. 332-348.

[20] Datta, S., Pratihar, D.K. and Bandyopadhyay, P.P., (2013). Modeling of plasma spray coating process using statistical regression analysis. *The International Journal of Advanced Manufacturing Technology*, *65*, pp. 967-980.

Qasim Abdulameer Sachit (corresponding author)
ORCID ID: 0009-0003-8119-9620
Production Engineering and Metallurgy Department
University of Technology, Iraq
Baghdad, Iraq
e-mail: pme.20.04@grad.uotechnology.edu.iq

Maan Abed Tawfiq
Production Engineering and Metallurgy Department
University of Technology, Iraq
Baghdad, Iraq
e-mail: Maan.A.Tawfiq@uotechnology.edu.iq

Osam Hassan Attia
ORCID ID: 0000-0002-2326-694X
Department of Reconstruction and Project
University of Baghdad
Baghdad, Iraq
e-mail: Osamhsattia@uobaghdad.edu.iq

Mohanad Jameel Zghair
Midland Refineries Company
Ministry of Oil
Baghdad, Iraq
e-mail: mohanadjameel@gmail.com